JOURNAL OF Materials CHEMISTRY

Synthesis conditions for hexagonal mesoporous silica layers†

Michaela Klotz, André Ayral, Christian Guizard and Louis Cot

Laboratoire des Matériaux et Procédés Membranaires, UMR 5635, CNRS, ENSCM, UMII, 8, rue de l'Ecole Normale, 34296 Montpellier cedex 5, France. E-mail: ayral@cit.enscm.fr

Received 30th July 1999, Accepted 1st December 1999

Hexagonal mesoporous silica layers were prepared by the sol–gel route using silicon alkoxides as silica precursors and alkyltrimethylammonium bromides to form the templating liquid crystal mesophase. The synthesis conditions required to obtain well-ordered crack-free layers were investigated. Thin layers exhibiting these properties were deposited from diluted sols. X-Ray diffraction enabled characterisation of the thermal evolution of their ordered structure and crystalline texture. Their porosity was experimentally measured from nitrogen adsorption–desorption analyses carried out directly on the thin layers. Two main synthesis parameters were identified. The first is the ageing time of the sol before deposition: ^{29}Si NMR showed that the disappearance of the ordered structure in the layers is related to the appearance of the Q_3 species in the sol. The second important synthesis parameter is the surfactant volume fraction in the medium after the removal of the volatile components. Using hexadecyltrimethylammonium bromide, well-ordered hexagonal layers were obtained for surfactant volume fractions ranging from 0.5 to 0.65, as expected from the corresponding water–surfactant binary diagram. For surfactants with shorter alkyl chains, the domain of existence of the hexagonal layers shifts to higher surfactant volume fractions in agreement with the evolution previously observed on the water–surfactant binary diagrams.

The synthesis of mesoporous molecular sieves using the templating effect of lyotropic liquid crystal mesophases was first proposed in 1992.[1,2] Aluminosilicate and silica particles were prepared by hydrothermal synthesis in the presence of cationic surfactants. Monnier *et al.*[3] suggested that the co-operative process of oxide polymerisation and mesophase formation was related to electrostatic interactions between the polar head of the surfactant molecules and the growing silicate oligomers. The synthesis of silica networks in ordered amphiphilic media was then carried out *via* sol–gel routes at room temperature and atmospheric pressure. It was also extended to the use of other kinds of amphiphilic molecules, *i.e.* neutral surfactants[4,5] and block-copolymers.[6,7]

A phase separation usually occurs in the synthesis solutions giving rise to individual particles of ordered oxide. Investigations were carried out in order to extend these synthetic methods to include the preparation of layers. Focusing on silica using alkyltrimethylammonium halides as surfactants, various types of layers and synthetic methods can be distinguished: self-supported thick layers obtained by interfacial reaction[8,9] or by casting of gelling solutions,[10] supported thin layers prepared by growth at the substrate–solution interface[11–13] or by deposition of gelling solutions. In the last case, mesophase-templated silica layers exhibiting lamellar,[14,15] hexagonal[15–18] and cubic structures[18] were obtained. The resulting porous layers are not always crack-free and sometimes extra-porosity can be observed on a larger scale than that of the ordered porosity produced by the templating mesophases.[19,20]

This work deals with the sol–gel preparation of supported hexagonal porous silica films. Our approach was defined from requirements associated with the expected applications as separative membranes or sensors. In such cases, a crack-free layer with a porosity which is limited to the ordered porosity generated by the crystalline template must be obtained. Moreover, our interest specifically concerns pore sizes located in the nanometer range. This requirement leads us to consider shorter length surfactant molecules than the hexadecyltrimethylammonium salts which are used in the majority of the studies reported in the literature.

In this paper, two approaches are successively evaluated for the preparation of hexagonal silica films from silicon alkoxides and alkyltrimethylammonium bromides. Analysis of the results enables determination of the synthetic conditions leading to crack-free hexagonal porous layers.

Experimental

Synthesis

The silica precursors used were silicon alkoxides (purity > 98%): tetramethoxysilane (TMOS) or tetraethoxysilane (TEOS). The surfactants employed were alkyltrimethylammonium bromides (purity > 98%): $C_nH_{2n+1}(CH_3)_3N^+Br^-$, with $n = 8$, 10, 12, 14 or 16, denoted as C_n. Distilled water, methanol or ethanol (purity: 99.8%) was also used to prepare the gelling sols.

Three types of sols, A, B and C, can be distinguished. Their compositions are summarised in Table 1. The preparation of these sols involved two steps: initially a gelling solution, G, was obtained by mixing the Si alkoxide with alcohol and acidic water (pH 2 from HCl addition). For A samples, the pH of solution G was then increased to 4 by addition of 0.1 M NH_3 solution. The second step involved addition of the surfactant, C_n, to solution G under stirring. In the cases of A and B samples, the surfactant was added immediately after the preparation of solution G. For the C samples, surfactant addition was carried out after a time, t_h, ranging from 0 to 400 min.

The sols were deposited as thin layers (TL) on flat glass substrates by dip coating and on tubular porous alumina substrates by slip casting. Deposition of the A and B sols was carried out immediately after their preparation. For the C sols, an ageing time, t_a, was applied before the deposition.

To obtain large quantities of sample, gelling solutions were poured into wide beakers, resulting in cracked thick layers

†Supplementary data available: calculation of the wall density and calculation of the surfactant volume fraction from the surfactant weight percentage. For direct electronic access see http://www.rsc.org/suppdata/jm/a9/a906181i/.

Table 1 Sol compositions

Sol	Alkoxide	Alcohol	Molar ratios in solution G alkoxide : H_2O : alcohol	Weight% of surfactant in the sol	pH
A	TMOS	Methanol	1 : 32.1 : 0.2	21	2–4
B	TMOS	Methanol	1 : 8.2 : 6.5	3.5–27	2
C	TEOS	Ethanol	1 : 8.2 : 6.75	3.4–14	2

(CL). For the A sols, monolithic wet gels were prepared in closed vessels and then dried immediately after gelation (UG) or aged for 4 d at 50 °C after gelation before drying (AG).

The samples were first dried at room temperature for 12 h and then for 2 h at 100, 150 and 175 °C in an oven. The thermal treatment effecting the removal of the surfactant was carried out up to 450 °C under nitrogen.

Characterisation

The condensation of the silica network in the sols and the gels was studied from liquid and magic angle spinning ^{29}Si NMR measurements, respectively. Methods allowing the quantitative comparison of the areas of the different Q_i peaks were applied (i being the number of bridging oxygen atoms of the SiO_4 tetrahedra).

The structural characterisation of the samples was undertaken using a low angle X-ray diffractometer with Cu-Kα radiation. The structural evolution *versus* temperature was followed in the $\theta/2\theta$ mode, 2θ varying from 1.2 to 9°. In the case of the unaged or aged A gels, the samples were sheared on a flat substrate prior to X-ray analysis. For the thin layers, samples deposited on glass slides were used. The crystalline texture of the layers was analysed with a fixed incidence angle mode. For fixed incidence angles α ranging from 0.025 and 5°, the analyser rotated between 1.5 and 3.5° in 2θ (the angle between the incident and diffracted beams).

The porous texture of the thermally treated samples was measured using nitrogen adsorption–desorption isotherms at 77 K. The pore size distribution in the mesoporosity range was estimated by analysis of the adsorption and desorption curves using the BJH method[21] and assuming cylindrical pores. For the thin layers deposited on glass slides, specific conditions were applied which are detailed in ref. 22.

The samples were observed by scanning electron microscopy (SEM) and transmission electron microscopy (TEM). For TEM analyses, microtomed slides of samples embedded in a polymer resin were used.

Results and discussion

Surfactant concentrated A sols

We first prepared A sols containing a weight percentage of surfactant equal to 21%. Considering the water–surfactant binary phase diagrams[23] (Fig. 1), it appears that this composition is located in an isotropic region near the boundary with the hexagonal mesophase domain. The formation of the mesophase can be explained in this case by a co-operative process.[3] Previous results[15,24] show that, under these conditions, the formation of the bidimensional hexagonal *P6mm* structure is observed for the shortest surfactant lengths, C_8 and C_{10}. However these amphiphilic molecules are less likely to self-associate than surfactants with longer alkyl chains, *e.g.* C_{16}, and the preservation of the crystalline structure is difficult.[25] Moreover, for composition A, the silica content is low, giving rise to the growth of a tenuous silica network in the aqueous phase of the hexagonal structure. We tried to increase the degree of condensation and hence the strength of the silica network by increasing the pH of the sol and by ageing the wet gels before the drying step. These experiments were carried out on sols synthesised with octyltrimethylammonium bromide (C_8).

Wet gels. ^{29}Si MAS NMR showed that both the increase in pH of the sols and ageing of the wet gels induces a significant increase in the Q_4 species at the expense of the Q_3 species. These results confirm the favourable effect of increasing the sol pH on the strengthening of the inorganic network. The wet gels exhibited a diffraction peak for $d = 24.5$ Å, corresponding to the (100) planes of the hexagonal phase for this surfactant.[26,27]

Thermally treated gels. For the various prepared samples, the diffraction peak associated with the ordered mesophase disappeared, except for the layers synthesised at pH 2. In this case the diffraction peak was broad [width at half maximum (in

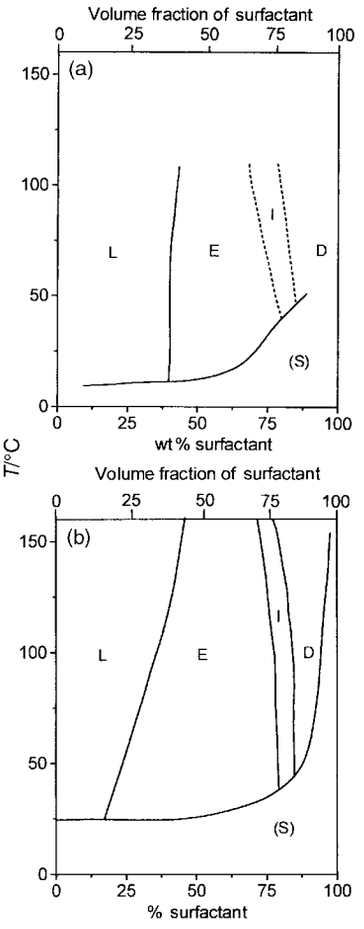

Fig. 1 (a) phase diagram of the water–tetradecyltrimethylammonium bromide system; (b) phase diagram of the water–hexadecyltrimethylammonium bromide system: L is the solution phase, E, I, and D are hexagonal, cubic, and lamellar liquid crystalline phases, respectively and (S) is solid surfactant. From the original diagrams,[23] a second abscissa axis (upper axis) is added corresponding to the volume fraction of surfactant. This parameter was calculated from the weight percentage of surfactant and the densities of water and surfactant at 20 °C. Reproduced with permission from ref. 23.

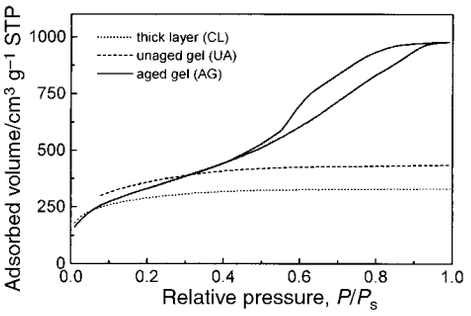

Fig. 2 Nitrogen adsorption–desorption curves for samples CL, UG and AG prepared with sol A and a final pH of 4.

$\theta) = 1°$] and of low intensity. This result can be attributed to the presence of very small ordered domains.[15] The estimated size of the ordered domains, applying the Scherrer formula,[28] is around 160 Å.

Fig. 2 shows the typical isothermal curves obtained for thick layers (CL) and unaged (UG) and aged (AG) gels prepared at pH 4. The main porosity characteristics are reported in Table 2. All the samples exhibit a very high specific surface area related to the presence of an important microporosity, evidenced by the high adsorbed volumes at low relative pressures (Fig. 2). The isotherms of CL and UG samples are of type I,[21] associated with mainly microporous materials. For AG samples, type IV isotherms[21] are obtained, exhibiting a hysteresis loop induced by the presence of mesoporosity. For the aged gel prepared at pH 4, the mesoporosity corresponds to about 60% of the porosity and the total porosity is very high, about 77%, based on a theoretical SiO_2 skeletal density of 2.20 g cm^{-3} (Table 2). These two levels of porosity, microporosity within the polymeric silica clusters and mesoporosity between clusters, are usually observed in the case of conventional two-step acid–base-catalysed silica xerogels.[29]

Surfactant diluted sols B and C

Using the results reported above, we modified the synthetic strategy by decreasing the relative percentage of surfactant and increasing the silicon alkoxide content in the initial sol. This approach is more specifically adapted to those layers for which the drying after deposition increases the concentration of the sol before gelation by removal of the volatile compounds (alcohol and water). The formation of the mesophase is mainly associated with surfactant enrichment of the medium. This method was previously applied with success by Ogawa[16] and Lu *et al.*[18]

We will first focus on the results obtained for a given weight percentage of C_{16} surfactant (9.3%) and then extend this to results allowing the discussion of the effect of the composition and the length of the surfactant molecule.

Study of sols B and C with 9.3 wt% of C_{16}. Images of crack-free thin layers obtained from this composition and deposited on dense or porous substrates are given in Fig. 3.

Fig. 4 shows the evolution *versus* temperature of the X-ray patterns for thin layers obtained from a B sol (TMOS as silicon

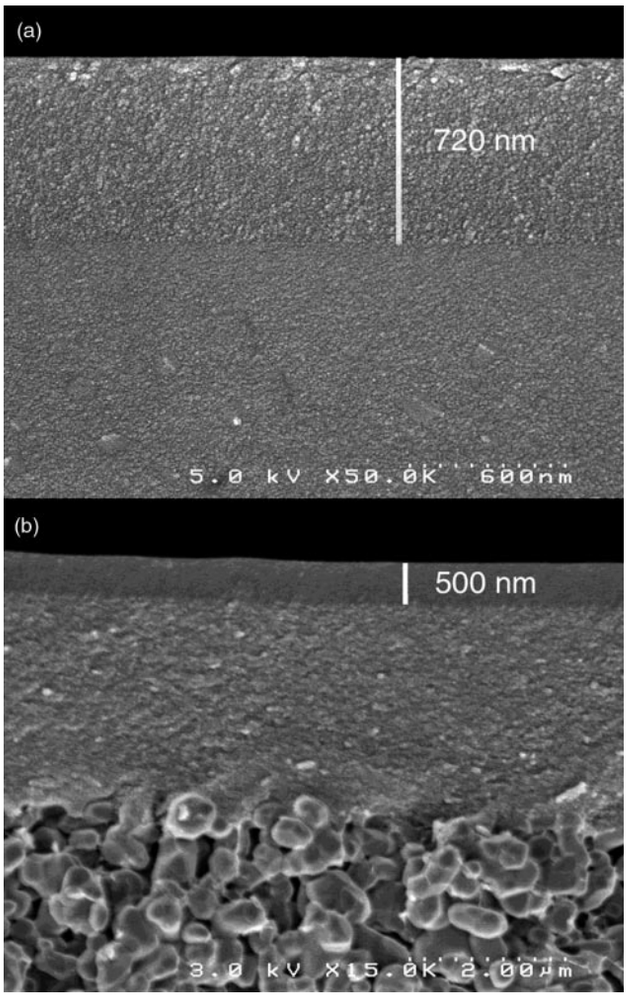

Fig. 3 SEM images of thin layers prepared from sol C [wt% (C_{16}) = 9.3, t_h = 60 min and t_a = 120 min]: (a) thin layer deposited on a dense glass substrate; (b) thin layer deposited on a mesoporous alumina layer (pore size of the top layer = 5 nm).

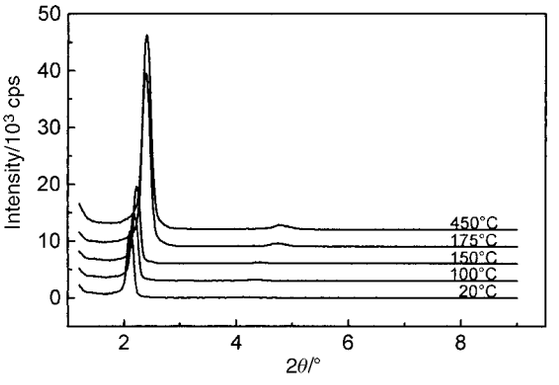

Fig. 4 Evolution of the diffraction pattern as a function of the treatment temperature for a thin layer [sol B, wt% (C_{16}) = 9.3].

Table 2 Characteristics of the porous texture for samples prepared from sol A (S_{BET} and $S_{Langmuir}$, specific surface areas measured applying the BET and Langmuir methods,[21] respectively; V_P, total pore volume)

Nature	pH	S_{BET}/m^2 g^{-1}	$S_{Langmuir}$/m^2 g^{-1}	V_P/cm^3 g^{-1}	Porosity P (%)	Microporosity (% of P)
CL	2	877	1230	0.45	50	96
	4	983	1420	0.51	53	93
UG	2	935	1320	0.48	51	95
	4	1249	1820	0.67	60	90
AG	2	1093	1510	0.61	57	85
	4	1223	1840	1.51	77	40

alkoxide). The main diffraction peak for the sample dried at 20 °C is located at $d_{20\,^{\circ}C}=40.5$ Å, and corresponds to the (100) planes of the hexagonal structure for C_{16}.[27,30] When the drying temperature is increased to 175 °C, a shift of the peak is observed: $d_{175\,^{\circ}C}=36.2$ Å. This shrinkage can be explained by the removal of residual water contained in the inorganic walls of the hexagonal structure and by supplementary condensation between neighbouring silanol groups.[29] The evolution of the Bragg spacing from 175 to 450 °C is low, around 0.2 Å. The peak width does not vary significantly with the temperature and the calculated size of the ordered domains is around 1000 Å. The diffracted intensity is dependent on the temperature (Fig. 4): a strong increase is observed between 150 and 175 °C prior to the departure of the surfactant, which is attributed to an increase in the sharpness of the interface between the micellar cylinders and the inorganic walls, associated with the loss of the residual water.

Only two peaks, d_{100} and d_{200}, are observed in the patterns of the thin layers (Fig. 4). This result can be explained by an alignment of the micellar cylinders along the substrate plane.[12] The alignment was evaluated from X-ray experiments at fixed incidence angle α. Fig. 5 shows the variations of the diffracted intensity *versus* α and 2θ for a layer dried at 20 °C and a layer thermally treated up to 450 °C. In each case, a strong maximum is observed for $\alpha=\theta_{100}$, corresponding to the expected diffraction angle for (100) planes parallel to the substrate surface. In the case of thick layers, the powder patterns present a broad diffraction peak.

Examples of TEM images observed for calcined thin (TL) or thick (CL) layers are given in Fig. 6. Characteristic honeycomb structures can be seen [Fig. 6(a)] and also alignments of parallel

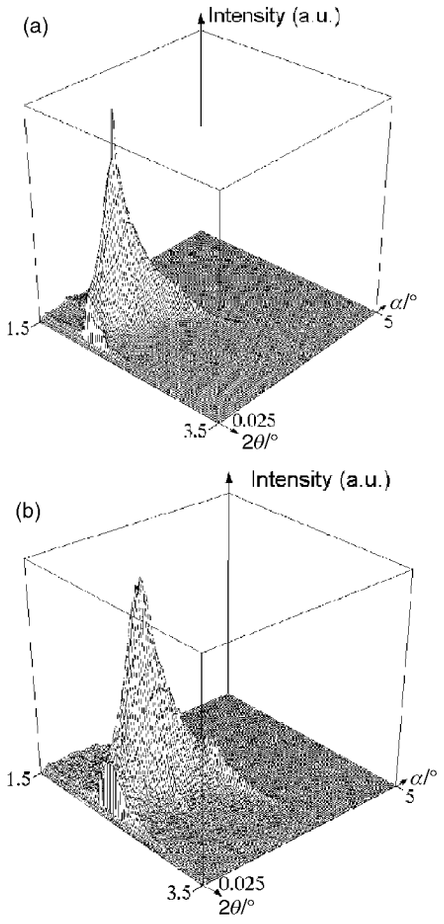

Fig. 5 Analysis of the crystalline texture for a thin layer [sol B, wt% (C_{16}) = 9.3]: (a) 20 °C; (b) 450 °C.

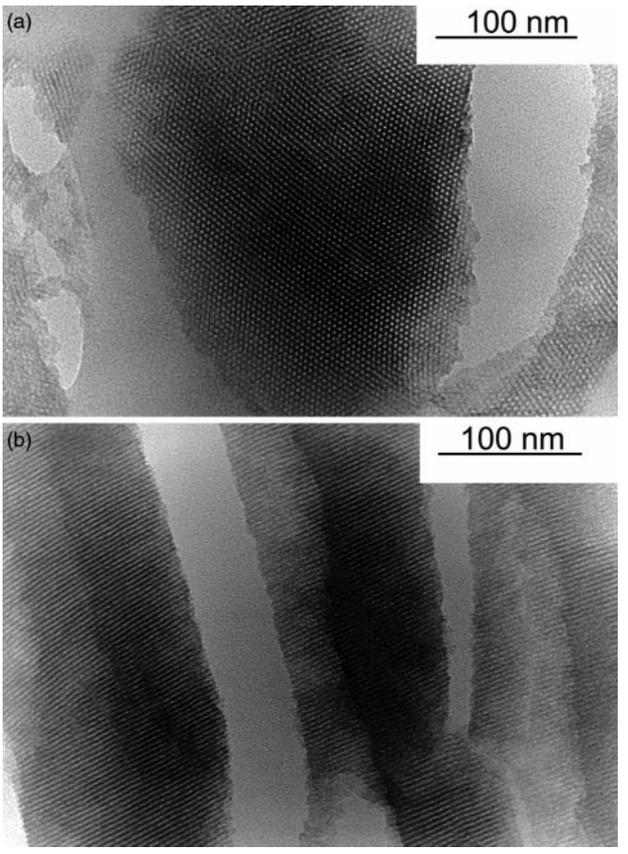

Fig. 6 TEM images of calcined thick layers (a) and thin layers (b) [sol B, wt% (C_{16}) = 9.3].

tubes [Fig. 6(b)]. This second type of image is the most frequently observed for the thin layers.

The porous texture of the layers obtained from sols B (TMOS) and C (TEOS) was characterised by nitrogen adsorption (Table 3). The isotherms for layers TL and CL of type B are given in Fig. 7. The two curves exhibit the same characteristic step associated with capillary condensation in the cylindrical pores. This phenomenon occurs at a relative pressure, P/P_s, of about 0.35, as expected using C_{16}.[30] The absence of a hysteresis loop can be explained by pore sizes of less than 3.6–3.8 nm.[31] The mean pore diameters determined by the BJH method from both adsorption and desorption curves are equal, as expected for pores with the same shape as the selected cylindrical model. The corresponding values, d_{BJH}, are reported in Table 3. The absence of extra-porosity at a larger scale can be deduced by the flatness of the curves for larger relative pressures. The first part of the isothermal curves enables us to estimate the microporosity existing in the silica walls. The calculation method is detailed in the supplementary material. The wall densities ρ_w obtained for the thin layers B and C are equal to 1.75 and 1.69 g cm^{-3}, respectively, values which can be compared to the bulk density of dense amorphous silica, 2.20 g cm^{-3}. From the Bragg spacing, d_{100}, and the volume fraction of the cylindrical pores, it is possible to calculate the diameter d_c of the cylindrical pore using Luzzati's formula[32] (see ESI). The theoretical surface area, S_t, developed by the cylindrical pores can also be estimated using the calculation method detailed in the supplementary material. The thickness of the silica walls, e, can be evaluated from the lattice parameter of the hexagonal structure, $a=2d_{100}/\sqrt{3}$ and the calculated diameter, d_c: $e=a-d_c$.

The use of TEOS, which is less reactive than TMOS,[29] enabled study of the effect of the hydrolysis time (before surfactant addition), t_h, and the ageing time (after surfactant addition) on the structure of the resulting thin layers. Fig. 8(a)

Table 3 Characteristics of the porous texture for samples prepared from sol B [wt% (C_{16}) = 9.3] and sol C [wt% (C_{16}) = 9.3, t_h = 60 min and t_a = 120 min]. The various parameters are defined in the text or in the supplementary material

Sol	Nature	S_{BET}/m^2 g^{-1}	V_p/cm^3 g^{-1}	P/P_s*	d_{BJH}/Å	d_{100}/Å	a/Å	ρ_w/g cm^{-3}	d_c/Å	e/Å	S_t/m^2 g^{-1}
B	TL	910	0.61	0.20	24	35	41	1.75	29	12	429
	CL	882	0.69	0.28	28	47	54	1.43	36	19	301
C	TL	836	0.61	0.20	24	38	44	1.69	31	13	382
	CL	718	0.53	0.28	28	55	64	1.44	36	28	216

shows that the main parameter is the time of ageing after hydrolysis and before deposition, *i.e.* $t_h + t_a$. For the various t_h values tested, the diffracted intensity always presents a maximum for $t_h + t_a$ equal to about 200 min and no further diffraction peaks are observed for $t_h + t_a > 400$ min. If we consider the evolution *versus* time of the area of the Q_i peaks in the ^{29}Si NMR spectra of a C sol [Fig. 8(b)], it appears that the maximum in the diffracted intensity corresponds to the predominance of Q_1 species in the sol and that the disappearance of the ordered mesophase is related to the appearance of Q_3 species in the sol. Thus, we can conclude that too large a condensation of the silica oligomers prevents the formation of the ordered phase.

Effect of the C_{16} content on the structure of the thin layers. From the previous results, we decided to define the surfactant content in the sols differently. Rather than the weight percentage in the starting sol, this content will be expressed by the volume fraction of surfactant in the material after elimination of the solvents and by-products, assuming that the silica phase exhibits a density equal to the wall density previously determined (1.75 and 1.69 g cm^{-3} for TMOS and TEOS, respectively). The details of the conversion method are given in the supplementary information. The main interest for the use of this new parameter is that it allows direct discussion of the conditions for preparation of hexagonal thin layers in terms of domain of existence of the hexagonal phase in the corresponding water–surfactant binary diagrams (Fig. 1).

Fig. 9(a) and 9(b) show the evolution of the diffracted intensity and the value of the Bragg spacing, d_{100}, as a function of the volume fraction of C_{16}. The diffracted intensity shows a maximum for a C_{16} volume fraction equal to 0.57 (corresponding to 9.3 wt% in the sol). Moreover, the sharpness of the peaks increases with the diffracted intensity. Three domains can be defined as a function of the C_{16} volume fraction. For volume fractions lower than 0.5 or higher than 0.65, weak and broad peaks are observed. Between these two limits, the hexagonal structure is well defined and maintained after calcination.

The limits of the hexagonal phase at 100 and 150 °C in the H_2O–C_{16} binary diagram [Fig. 1(b)] are reported in Fig. 9(a). It clearly shows that the domain of well-ordered hexagonal silica layers is located and centred between these limits.

The Bragg spacing, d_{100}, increases as the C_{16} volume fraction decreases [Fig. 9(b)]. This phenomenon can be explained by a swelling of the structure associated with an increase in the volume fraction of the aqueous phase. Moreover, when the temperature of the final treatment was increased, a contraction of the structure was observed which is related to shrinkage of the silica network. This shrinkage is a maximum for the highest C_{16} volume fractions, and hence the lowest silica contents.

For C sols (TEOS), similar behaviour was observed with a slight shift of the domain of well-ordered hexagonal silica layers to lower surfactant volume fractions (Fig. 10). Previous results on water–alcohol–surfactant ternary diagrams[33,34] showed that the location of the hexagonal mesophase domain depends on the nature and amount of the added alcohol. However, it must also be noted that the X-ray diffraction results obtained with B or C sols were clearly confirmed with several other sols more diluted by alcohol or with higher water–alkoxide molar ratios, but with an equivalent C_{16} volume fraction (which depends on the surfactant–silicon alkoxide molar ratio and on the wall density (see ESI). Moreover, from the surfactant–silicon alkoxide molar ratios reported in the literature for sols leading to hexagonal layers,[16–18] the corresponding surfactant volume

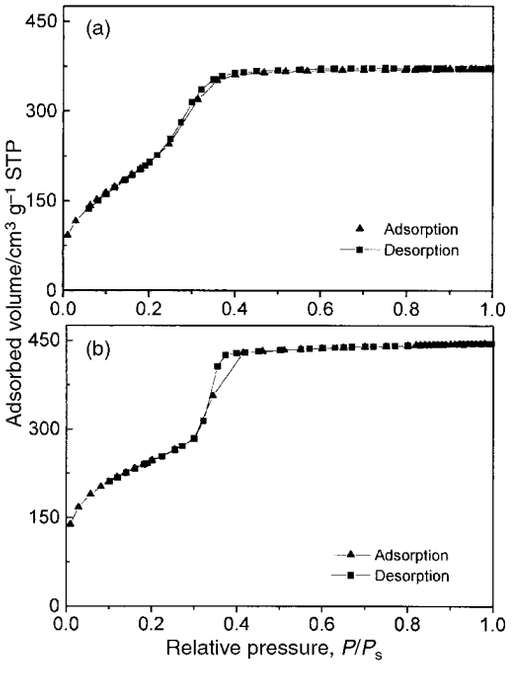

Fig. 7 Nitrogen adsorption–desorption curves for calcined layers [sol B, wt% (C_{16}) = 9.3]: (a) thin layer TL; (b) thick layer CL.

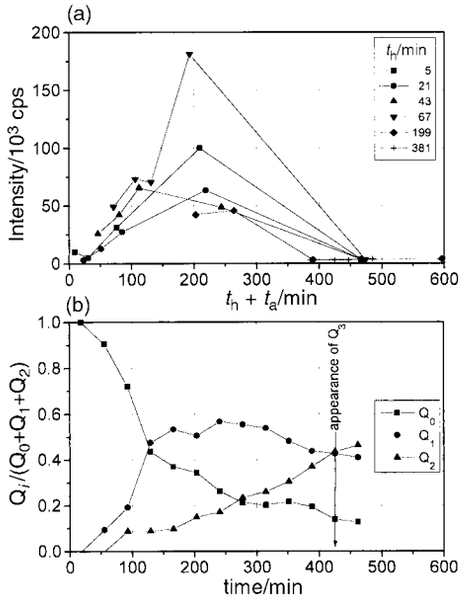

Fig. 8 (a) Variation of the diffracted intensity of the (100) peak as a function of the total ageing time ($t_h + t_a$) for different values of t_h [sol C, wt% (C_{16}) = 9.3]. (b) Evolution *versus* time of the Q_i species in a C sol [wt% (C_{16}) = 9.3, t_h = 5 min].

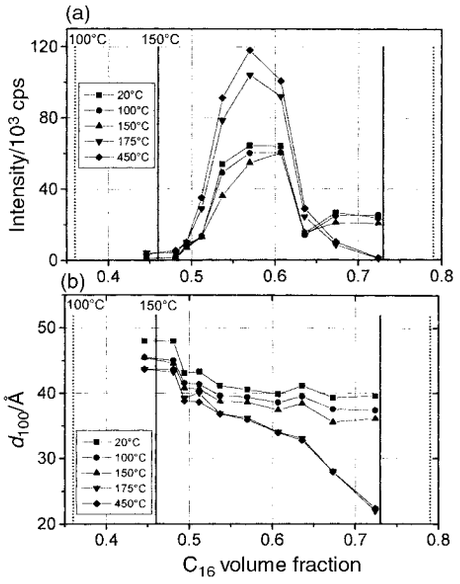

Fig. 9 Variation, *versus* C_{16} volume fraction, of (a) the diffracted intensity and (b) the Bragg spacing, d_{100} , for a B sol.

fractions were calculated, assuming a wall density equal to 1.75 g cm^{-3}. Except for the lowest surfactant–silicon alkoxide molar ratio in ref. 17, the resulting values are also located in the hexagonal domain of the water–hexadecyltrimethylammonium bromide [Fig. 1(b)] or water–hexadecyltrimethylammonium chloride[35] diagrams.

Effect of the composition and the surfactant alkyl chain length. The study carried out for hexadecyltrimethylammonium bromide was extended to surfactants with shorter alkyl chains. The evolution of the diffracted intensity *versus* volume fraction of surfactant C_n ($n=8$, 10, 12, 14 and 16) is reported in Fig. 11 for two temperatures of final treatment: 20 and 450 °C. The domain of existence of the hexagonal phase shifts to higher surfactant volume fractions when n decreases. This result is in agreement with the evolution observed on the water–alkyltrimethylammonium halides binary diagrams[36] for bromides[23] or chlorides.[33,35,37] On the other hand, the

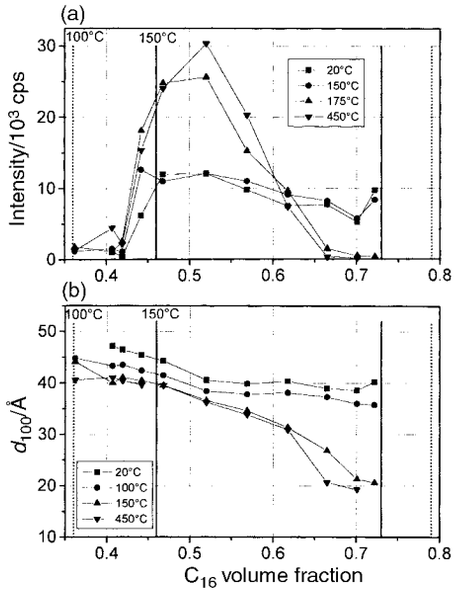

Fig. 10 Variation, *versus* C_{16} volume fraction, of (a) the diffracted intensity and (b) the Bragg spacing, d_{100}, for a C sol ($t_h=60$ min and $t_a=120$ min).

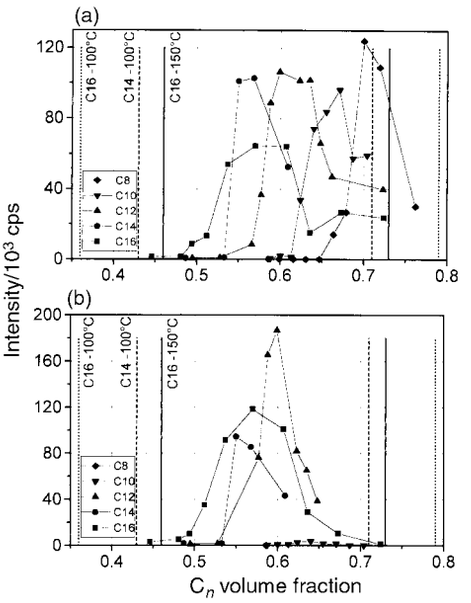

Fig. 11 Variation, *versus* C_n volume fraction, of the diffracted intensity for a B sol: (a) thin layer dried at 20 °C; (b) thin layer calcined at 450 °C.

hexagonal structure of the calcined layers disappears progressively for C_n volume fractions larger than about 0.65. Well ordered porous layers are obtained only for the higher n values, $n=12$, 14 and 16.

The variation of the Bragg spacing d_{100} *versus* surfactant volume fraction for the different values of n, is shown in Fig. 12. It appears that tailoring of the pore size and of the porosity in the thin layers is possible by modifying the surfactant chain length or the sol composition. For instance, for a C_{12} volume fraction equal to 0.6, d_c is equal to 21 Å.

Conclusion

Hexagonal silica layers were prepared from silicon alkoxides and alkyltrimethylammonium bromides. The use of surfactant-diluted sols enabled the production of crack-free silica layers exhibiting a well-ordered hexagonal mesoporosity. In this case, the mechanism of formation of the templating mesophase is mainly the concentration of the starting sol after deposition by fast evaporation of the volatile components. The ageing time of the sol must be short enough to limit polymerisation of the silica network prior to the deposition. As a matter of fact, the reticulation of the silica network disfavours concentration of the sol, which is required to obtain hexagonal packing of the micellar cylinders. An important parameter used to evaluate the ability of the sols to form hexagonal layers is the surfactant volume fraction in the medium after removal of the volatile components. From this parameter, and using the water–surfactant binary phase diagrams, it is possible to define the

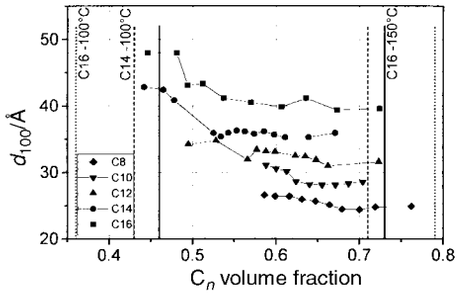

Fig. 12 Variation, *versus* C_n volume fraction, of d_{100} (sol B; thin layer dried at 20 °C).

chemical compositions of the starting sols. When the length of the alkyl chain decreases, the amount of surfactant required to form the hexagonal phase increases. On the other hand, if the surfactant content in the deposited layer is too high, the hexagonal structure disappears during the thermal treatment applied to eliminate the templating mesophase. Thus, well-ordered porous layers are obtained only for the surfactants exhibiting the longest alkyl chains (hexadecyl, tetradecyl and dodecyl).

References

1 C. T. Kresge, M. E. Leonowicz, W. J. Roth, J. C. Vartuli and J. S. Beck, *Nature*, 1992, **359**, 710.
2 J. S. Beck, J. C. Vartuli, W. J. Roth, M. E. Leonowicz, C. T. Kresge, K. D. Schmitt, C. T.-W. Chu, D. H. Olson, E. W. Sheppard, S. B. McCullen, J. B. Higgins and J. L. Schlenker, *J. Am. Chem. Soc.*, 1992, **114**, 10834.
3 A. Monnier, F. Schüth, Q. Huo, D. Kumar, D. Margolese, R. S. Maxwell, G. D. Stucky, M. Krishnamurty, P. Petroff, A. Firouzi, M. Janicke and B. F. Chmelka, *Science*, 1993, **261**, 1299.
4 P. T. Tanev and T. J. Pinnavaia, *Science*, 1995, **267**, 865.
5 S. A. Bagshaw, E. Prouzet and T. J. Pinnavaia, *Science*, 1995, **269**, 1242.
6 M. Templin, A. Franck, A. Du Chesne, H. Leist, Y. Zhang, R. Ulrich, V. Schädler and U. Wiesner, *Science*, 1997, **278**, 1795.
7 D. Zhao, P. Yang, N. Melosh, J. Feng, B. F. Chmelka and G. D. Stucky, *Adv. Mater.*, 1998, **10**, 1380.
8 H. Yang, N. Coombs, I. Sokolov and G. A. Ozin, *Nature*, 1996, **381**, 589.
9 H. Yang, N. Coombs, O. Dag, I. Sokolov and G. A. Ozin, *J. Mater. Chem.*, 1997, **7**, 1755.
10 M. Ogawa and T. Kikuchi, *Adv. Mater.*, 1998, **10**, 1077.
11 J. Liu, J. R. Bontha, A. Y. Kim and S. Baskaran, *Mater. Res. Soc. Symp. Proc.*, 1996, **431**, 245.
12 H. Yang, A. Kuperman, N. Coombs, S. Mamiche-Afara and G. A. Ozin, *Nature*, 1996, **379**, 703.
13 H. Yang, N. Coombs, I. Sokolov and G. A. Ozin, *J. Mater. Chem.*, 1997, **7**, 1285.
14 M. Ogawa, *J. Am. Chem. Soc.*, 1994, **116**, 7941.
15 T. Dabadie, A. Ayral, C. Guizard, L. Cot and P. Lacan, *J. Mater. Chem.*, 1996, **6**, 1789.
16 M. Ogawa, *Chem. Commun.*, 1996, 1149.
17 P. J. Bruinsma, N. J. Hess, J. R. Bontha, J. Liu and S. Baskaran, *Mater. Res. Soc. Symp. Proc.*, 1997, **443**, 105.
18 Y. Lu, R. Ganguli, C. A. Drewien, M. T. Anderson, C. J. Brinker, W. Gong, Y. Guo, H. Soyez, B. Dunn, M. H. Huang and J. I. Zinks, *Nature*, 1997, **389**, 364.
19 J. E. Martin, M. T. Anderson, J. Odinek and P. Newcomer, *Langmuir*, 1997, **13**, 4133.
20 M. T. Anderson, J. E. Martin, J. G. Odinek and P. Newcomer, *Mater. Res. Soc. Symp. Proc.*, 1996, **431**, 217.
21 S. Lowell and J. E. Shields, *Powder Surface Area and Porosity*, Chapman and Hall, London, 1984.
22 A. Ayral, A. El Mansouri, M.-P. Vieira and C. Pilon, *J. Mater. Sci. Lett.*, 1998, **17**, 883.
23 T. Warnheim and A. Jonsson, *J. Colloid Interface Sci.*, 1988, **125**, 627.
24 T. Dabadie, Ph.D. Thesis, University of Montpellier II, 1994.
25 J. S. Beck, J. C. Vartuli, G. J. Kennedy, C. T. Kresge, W. J. Rothand and S. E. Schramm, *Chem. Mater*, 1994, **6**, 1816.
26 A. Sayari, M. Kruk and M. Jaroniec, *Catal. Lett.*, 1997, **49**, 147.
27 P. I. Ravikovitch, D. Wei, W. T. Chueh, G. L. Haller and V. Neimark, *J. Phys. Chem. B*, 1997, **101**, 3671.
28 P. Scherrer, *Nachr. Göttinger Gesel. Dtsch.*, 1918, **2**, 98.
29 C. J. Brinker and G. W. Scherrer, *Sol–Gel Science. The Physics and Chemistry of Sol–Gel Processing*, Academic Press, San Diego, 1990.
30 M. Kruk, M. Jaroniec and A. Sayari, *J. Phys. Chem. B*, 1997, **101**, 583.
31 S. Inoue, Y. Hanzawa and K. Kaneko, *Langmuir*, 1998, **14**, 3079.
32 V. Luzzati, H. Mustacchi, A. Skoulios and F. Husson, *Acta Crystallogr.*, 1960, **13**, 660.
33 P. Ekwall, *Adv. Liq. Cryst.*, 1975, **1**, 1.
34 K. Fontell, A. Khan, B. Lindstrom, D. Maciejewska and S. Puang-Ngern, *Colloid Polym. Sci.*, 1991, **269**, 727.
35 U. Henriksson, E. S. Blackmore, G. J. T. Tiddy and O. Söderman, *J. Phys. Chem.*, 1992, **96**, 3894.
36 E. S. Blackmore and G. J. T. Tiddy, *J. Chem. Soc., Faraday Trans. 2*, 1988, **84**, 1115.
37 R. R. Balmbra, J. S. Clunie and J. F. Goodman, *Nature*, 1969, **22**, 1159.

Paper a906181i